JACS
JOURNAL OF THE AMERICAN CHEMICAL SOCIETY
pubs.acs.org/JACS
Article

Reversible Structural Isomerization of Nature's Water Oxidation Catalyst Prior to O–O Bond Formation

Yu Guo, Johannes Messinger,* Lars Kloo,* and Licheng Sun*

Cite This: *J. Am. Chem. Soc.* 2022, 144, 11736–11747
Read Online
ACCESS | Metrics & More | Article Recommendations | Supporting Information

ABSTRACT: Photosynthetic water oxidation is catalyzed by a manganese–calcium oxide cluster, which experiences five "S-states" during a light-driven reaction cycle. The unique "distorted chair"-like geometry of the $Mn_4CaO_{5(6)}$ cluster shows structural flexibility that has been frequently proposed to involve "open" and "closed"-cubane forms from the S_1 to S_3 states. The isomers are interconvertible in the S_1 and S_2 states, while in the S_3 state, the open-cubane structure is observed to dominate in *Thermosynechococcus elongatus* (cyanobacteria) samples. In this work, using density functional theory calculations, we go beyond the $S_3{}^{+}Y_z$ state to the $S_3{}^{n}Y_z{}^{\bullet} \rightarrow S_4{}^{+}Y_z$ step, and report for the first time that the reversible isomerism, which is suppressed in the $S_3{}^{+}Y_z$ state, is fully recovered in the ensuing $S_3{}^{n}Y_z{}^{\bullet}$ state due to the proton release from a manganese-bound water ligand. The altered coordination strength of the manganese–ligand facilitates formation of the closed-cubane form, in a dynamic equilibrium with the open-cubane form. This tautomerism immediately preceding dioxygen formation may constitute the rate limiting step for O_2 formation, and exert a significant influence on the water oxidation mechanism in photosystem II.

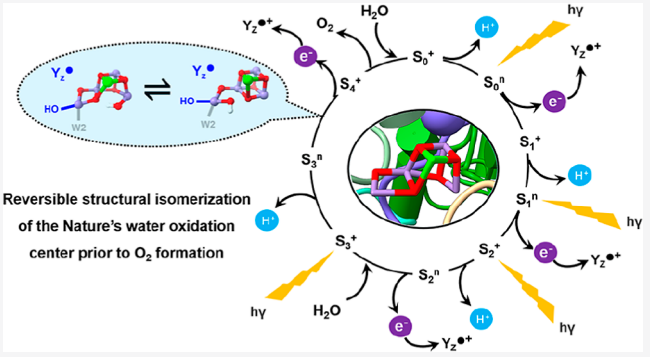

INTRODUCTION

Photosystem II (PSII) is a metalloenzyme that catalyzes water splitting to molecular oxygen in cyanobacteria, algae, and plants. It evolved about 3 billion years ago at the level of ancient cyanobacteria (Figure 1a). The embedded "oxygen-evolving complex (OEC)", composed of a Mn_4CaO_5 cluster surrounded by water and amino acid ligands (Figure 1b,c), acts as a highly efficient water oxidation catalyst. Due to charge separations in the reaction center of PSII, the OEC is initially stepwise oxidized during the cyclic catalysis, so that it attains four (meta)stable intermediates (S_0, S_1, S_2, and S_3) and one transient S_4 state, the latter of which initiates O_2 formation.[1−10] Accounting also for proton release and charge of the $Mn_4CaO_{5(6)}$ complex, the classical five-step "S-state cycle"[11] can be refined to instead include nine intermediate states that are separated by kinetically distinguishable proton and electron transfer steps (Figure 1d).[3,12−22]

Structural polymorphism of the OEC has been proposed and experimentally observed, mainly by electron paramagnetic resonance (EPR) spectroscopy, for some decades.[1,4,18,23−30] More recently, the first detailed theoretically models were proposed for interpreting these findings.[31,32] However, the proposed alternative structures have thus far eluded verification by structural methods such as protein crystallography.[33−40] The structural flexibility in the S_2 state is typically attributed to the mobile μ-oxo bridge (O5) between Mn1 and Mn4,[31,41] producing "open" (A) and "closed" cubane (B) forms of the cluster (Figure 1e, see supplementary references in the Supporting Information). As recently discovered by Pantazis and co-workers, orientational Jahn–Teller isomerism in the resting S_1 state[41] generates the precursors for the two interconvertible A and B structures of the S_2 state,[31] which give rise to the low-spin ($S = 1/2$) and high-spin ($S = 5/2$) EPR signals in plant PSII at $g = 2$ and $g \approx 4.1$, respectively, and the latter $g \approx 4.1$ (and similar signals around this value) can only be produced by mutations or chemical treatments in cyanobacteria.[42] These authors also proposed that the closed-cubane form is the entry to the S_3 state,[43,44] in agreement with molecular dynamics studies by Guidoni and co-workers.[32,45] This closed-cubane interpretation for the S_2 high-spin ($S = 5/2$) state is widely accepted in the field and consistent with the calculations in this report and will hence be employed in this study. However, we note that two competing interpretations exist. First, based on broken-symmetry density functional theory (BS-DFT) calculations with focus on spectroscopic parameter analysis, Corry and O'Malley proposed an isomer in

Received: April 6, 2022
Published: June 24, 2022

https://doi.org/10.1021/jacs.2c03528
J. Am. Chem. Soc. 2022, 144, 11736–11747

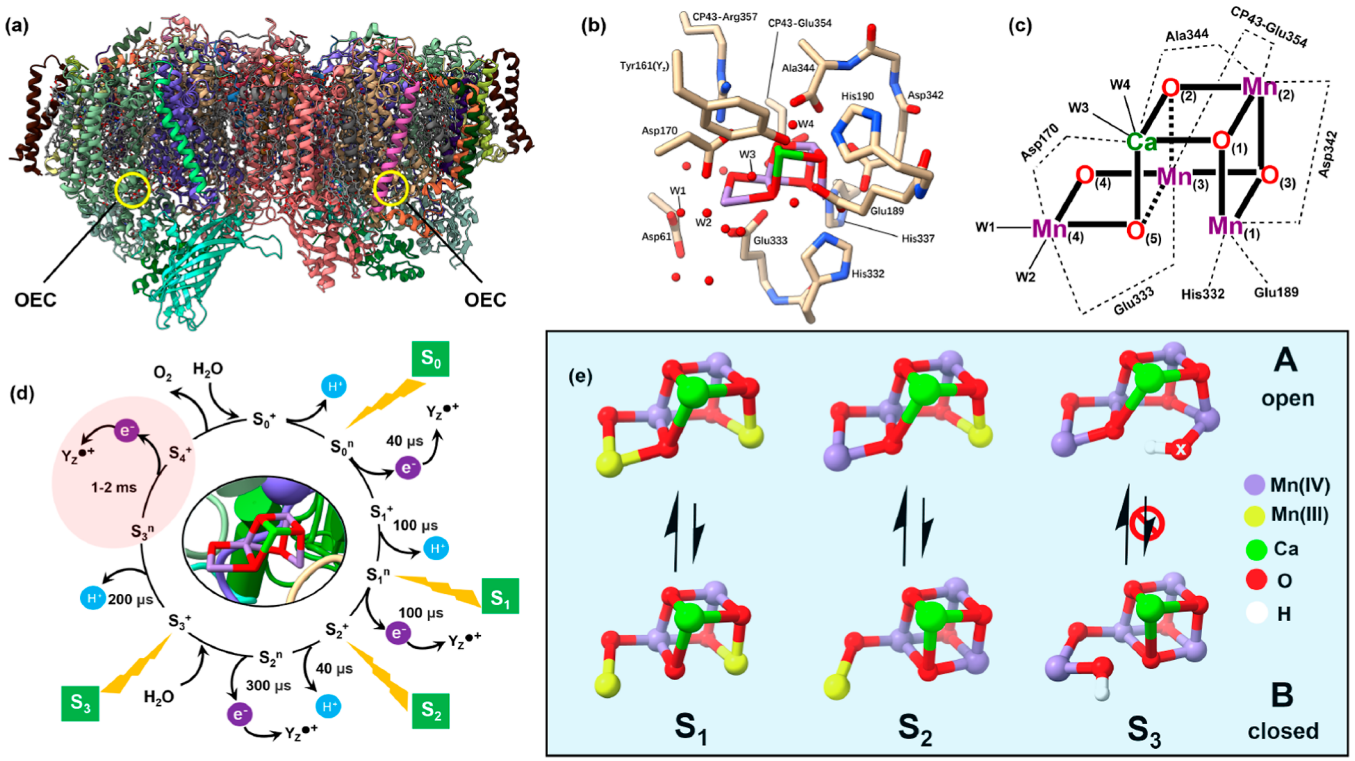

Figure 1. (a) View of PSII dimer and the OEC location from *Thermosynechococcus elongatus* (PDB ID: 6W1O)[38] (b) Mn_4CaO_5 cluster and its local surroundings in its dark-stable S_1 state. (c) Sketch map of atom labeling and connectivity of the first coordination sphere ligands in the Mn_4CaO_5 cluster. (d) Extended S-state cycle including nine intermediates with sequence of proton and electron transfer and kinetics between transitions;[3,13−15,17,21,22,70] the red phase is the main focus of this study. (e) Structural flexibility of the OEC cluster in the S_1, S_2, and S_3 states, marked with the reversibility between open (A) and closed (B) cubane structures (for references, see the main text).

the S_2 state by W1 deprotonation to μ-O4 to rationalize the high-spin (S = 5/2) form[46] and, on this basis, further identified a high-spin (S = 7/2) deprotonated intermediate with μ-hydroxo O4 during the $S_2 \rightarrow S_3$ transition, without invoking a closed-cubane structure.[47] Second, another model for the high-spin (S = 5/2) S_2 state assumes the early binding of a substrate water to Mn1 as OH^- originating from W3, as suggested by Siegbahn[48] and later by Pushkar et al.[49] For a detailed discussion of such models, see Text S6 in the Supporting Information.

The open-cubane S_3 structure contains an extra oxygen ligand to Mn1 due to binding of an additional water molecule. This was proposed first by Siegbahn on the basis of DFT calculations[50−53] that are found on the results from extended X-ray absorption fine structure (EXAFS) experiments,[54−56] showing that the S_2−S_3 transition involves the conversion of a five-coordinate Mn(III) to a six-coordinate Mn(IV). Cox et al. confirmed by advanced EPR that all Mn ions in the S_3 state are hexa-coordinate and that the "water-added" open-cubane S_3 structure, $S_3^{A,W}$ ("W" denotes the extra water binding), is consistent with their experimental data.[57] Isobe et al. constructed multiple S_3 models[58,59] that vary with regard to total spin and Mn-valence and proposed that the closed-to-open cubane transformation is possible in a stepwise process involving an oxyl−oxo precursor.[60] By contrast, Capone et al.[61] and Shoji et al.[62] showed different feasible pathways for a direct closed-to-open cubane conversion. Regardless of the mechanistic details, a consensus has been reached that the OEC cluster in the S_3 state (more precisely the $S_3{}^+Y_z$ state, see below) allows for unidirectional conversion from the water-added closed ($S_3^{B,W}$) to the open-cubane ($S_3^{A,W}$) form, but not vice versa (Figure 1e). $S_3^{B,W}$ (S = 3) is proposed to be the precursor form of the final $S_3^{A,W}$ (S = 3) under the pivot/carousel mechanism of water binding during the $S_2 \rightarrow S_3$ transition.[43,44,63] Importantly, the dominance of the open-cubane Mn core topology is consistent with the S_3 state structures resolved by serial crystallography using X-ray free electron lasers (XFELs).[35−38]

Nevertheless, alternative S_3 state models that assume early O−O bonding exist.[1,23,64] For example, Corry and O'Malley proposed a chemical equilibrium between "oxo-hydroxo" and "peroxo" for O5−Ox in the S_3 state, based on a comparison of experimental and BS-DFT calculated geometries and magnetic resonance properties.[65−67] In higher-plant PSII, a recent combined EPR and DFT study by Zahariou et al. provided evidence, in PSII isolated from spinach for S_3 being a mixed state of $S_3^{A,W}$ (S = 3) and $S_3^{B,unbound}$ (S = 6) ("unbound" denotes the unsaturated coordination of Mn4; "$S_3^{B,unbound}$" is used throughout to refer to the "S_3^B" in its original publication, and similarly $S_4^{B,unbound}$ for S_4^B).[68,69] Here, the dominant state (~80%) has been identified as the $S_3^{B,unbound}$ state, that is, a closed-cubane S_3 state with penta-coordinate Mn4(IV) without additional bound water. In this view, it should be emphasized that the structural isomerism in the S_3 state introduced here (and discussed later) should apply to that of cyanobacterial PSII, and the less populated S_3 form in higher plants.

Consistent with the abovementioned findings for the $S_3{}^+Y_z$ state, it is commonly assumed that the O−O bond formation in the S_4^+ state also occurs in the open-cubane ($S_4^{A,W}$) conformation.[4,35,37,51,53,57,71−79] However, there have been also several proposals based on a closed-cubane structure ($S_4^{B,W}$ or $S_4^{B,unbound}$),[4,68,69,73,75,80−87] which is in sharp contrast in terms

https://doi.org/10.1021/jacs.2c03528
J. Am. Chem. Soc. 2022, 144, 11736−11747

Scheme 1. Structural Isomerization between $S_3^{A,W}Y_z^{\bullet}$ (Left) and $S_3^{B,W}Y_z^{\bullet}$ (Right) in the $S_3{}^nY_z^{\bullet}$ (W1 = OH^-) State Explored in the Present Study[a]

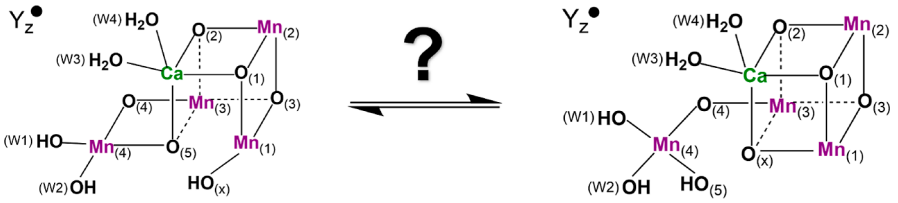

[a]Amino acid ligands are omitted for clarity.

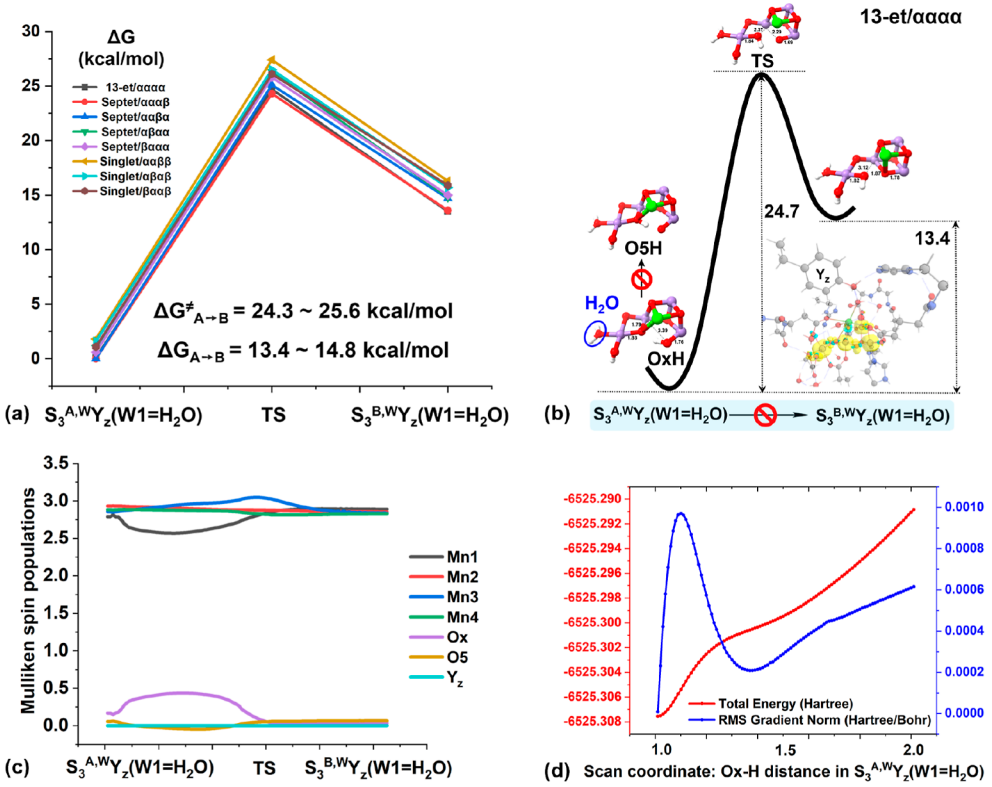

Figure 2. (a) Relative Gibbs free energy profiles for the conversion between $S_3^{A,W}Y_z(W1{=}H_2O)$ and $S_3^{B,W}Y_z(W1{=}H_2O)$ in all the possible spin states of the $S_3{}^+Y_z$ state. Because of the close similarity to the other spin states, more information regarding the changes of (b) geometric structures, (c) electronic configurations along the MEP, and (d) relaxed PES scan curve of proton transfer between Ox and O5 are exemplified in the highest 13-et/*αααα* spin state. Spin populations are displayed in yellow contours and key interatomic distances are given in Å.

of geometric configuration. This motivates us to investigate if structural heterogeneity exists just before the S_4^+ state is formed from the S_3^n state via electron abstraction by $Y_z^{\bullet}$. In this paper, we mainly focus on the possibility of structural isomerization in the $S_3{}^nY_z^{\bullet}$ states (Scheme 1), employing DFT calculations. The correlation of our results with experimental observations and the implications for the mechanism of O−O bond formation are discussed.

RESULTS AND DISCUSSION

Unidirectional Structural Isomerization in the $S_3{}^+Y_z$ State. Unlike the structural interconversion simply caused by O5 shuttling between Mn1 and Mn4 in the S_2 state (the most likely mechanism accounting for the EPR isomers, see Text S6 in the Supporting Information), isomerization in the $S_3{}^+Y_z$ state results from Mn3 ligand exchange between O5 and Ox. We revisited this process by our quantum chemical model (Figure S1 in the Supporting Information) and determined a direct conversion pathway connecting the open and closed-cubane structures. A notable phenomenon is that the incidental proton transfer is directed toward the moiety becoming a terminal ligand; protonation of the *μ*-oxo ligand is impossible in either isomer (O5H in $S_3^{A,W}$ or OxH in $S_3^{B,W}$), which is justified by the relaxed potential energy scan for proton translocation between Ox and O5 (Figure 2d, Text S1 in the Supporting Information).

In contrast to Capone et al.,[61] where the formal oxidation state of Mn3 is lowered from (IV) to (III), while Mn1 acquires a partial radical character in the proximity of the transition state (TS), our results show that the electronic configuration of the OEC cluster essentially remains constant along the minimum energy paths (MEPs). That means all Mn keep valence (IV) throughout as reflected by the Mulliken spin populations (Figure 2c, Text S2 and Table S2 in the Supporting Information). The reason may be attributed to the exclusion of structural and thermal fluctuations along the MEPs, which are instead present during the molecular dynamics simulations. Anyhow, consistent with Isobe et al.,[60]

https://doi.org/10.1021/jacs.2c03528
J. Am. Chem. Soc. 2022, 144, 11736−11747

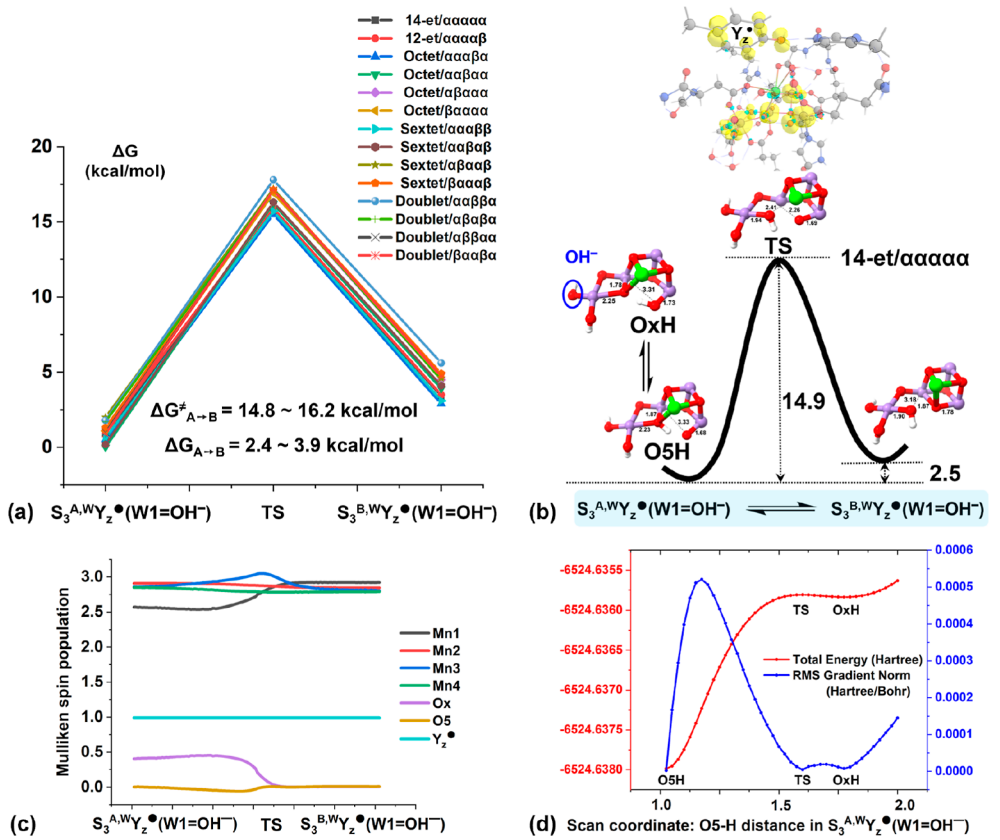

Figure 3. (a) Relative Gibbs free energy profiles for the conversion between $S_3^{A,W}Y_z^{\bullet}$(W1═OH^-) and $S_3^{B,W}Y_z^{\bullet}$(W1═OH^-) in all the possible spin states of the $S_3^{n}Y_z^{\bullet}$ state. Because of the close similarity to the other spin states, the highest 14-et/*αααααα* spin state was selected for visualizing more information regarding the changes of (b) geometric structures and (c) electronic configurations along the MEP, and (d) relaxed PES scan curve of proton transfer between Ox and O5.

our calculated $S_3^{A,W} \rightarrow S_3^{B,W}$ barriers of 24.3−25.6 kcal/mol and stabilization energies of 13.4−14.8 kcal/mol for the open-cubane form ($S_3^{A,W}$) on all the spin surfaces (Figure 2a,b, Table S1 in the Supporting Information) show that the same conclusion can be drawn, that is, conformational change in the $S_3^{+}Y_z$ state is essentially confined to the unidirectional closed-to-open cubane conversion and forbidden reversely. Consequently, the bidirectional structural flexibility prevalent in both S_1 and S_2 states has disappeared in the following $S_3^{+}Y_z$ state, with an overwhelming preference for the open-cubane structure.

It is worth mentioning that the abovementioned conclusion is strictly only valid for the $S_3^{+}Y_z$ state and does not apply for the $S_2^{+}Y_z^{\bullet}$ state, which can be formed from the $S_3^{+}Y_z$ state by electron back donation from Y_z to Mn under certain conditions, as shown in some experimental findings.[88−90] The structural equilibration in the $S_2^{n}Y_z^{\bullet}$ state was suggested as a requirement for water exchange in the $S_3^{+}Y_z$ state,[91] in which the open-to-closed conversion is involved and readily reversible, but necessitates a Mn(III) center within the cluster.

Reversible Structural Isomerization in the $S_3^{n}Y_z^{\bullet}$ State. By various experimental approaches, it has been established that O_2 formation and release begins after the flash-induced formation of the $S_3^{+}Y_z^{\bullet}$ state only after a lag phase of about 200 μs.[12,70−92] This lag phase has been assigned to a deprotonation reaction in the S_3^{+} to S_3^{n} transition, as shown in Figure 1d. Since the initial deprotonation site has been widely acknowledged as W1(H_2O) (via the egress gate Asp61 to the lumen) during the $S_3 \rightarrow S_4$ transition,[52,53,78,93−96] this ligand was formulated as a hydroxide (OH^-) in our $S_3^{n}Y_z^{\bullet}$ model, in agreement with a series of previous computational work.[52,53,94,96] In analogy to the abovementioned case of $S_3^{+}Y_z$, redox-related events were not observed at any of the Mn centers along the whole MEP (Figure 3c and Table S4 in the Supporting Information) and various spin couplings do not significantly affect the energetics even after $Y_z^{\bullet}$ addition. The redox-irrelevance and spin-insensitivity for such a ligand exchange are understandable because the octahedral coordination geometry of Mn3(IV) basically maintains during the simultaneous movements of O5 and Ox in opposite directions, and the two oxygens never approach a bonding distance to cause Mn reduction.

Interestingly, the obtained reaction landscapes of the structural isomerization in the $S_3^{n}Y_z^{\bullet}$ state is fundamentally changed with regard to both thermodynamics and kinetics (Figure 3a,b, Table S3 in the Supporting Information) as compared to that of the $S_3^{+}Y_z$ state (Tables S1 in the Supporting Information), allowing for a dynamically reversible isomerization $S_3^{A,W}Y_z^{\bullet} \rightleftharpoons S_3^{B,W}Y_z^{\bullet}$ in chemical equilibrium. First, the relative thermodynamic stability of $S_3^{B,W}Y_z^{\bullet}$ is greatly enhanced to only 2.4−3.9 kcal/mol higher in free energy than $S_3^{A,W}Y_z^{\bullet}$ (vs 13.4−14.8 kcal/mol in the $S_3^{+}Y_z$ state). Superficially, according to the relationship between ΔG° and equilibrium constant K, this energy difference would still correspond to a major population of $S_3^{A,W}Y_z^{\bullet}$ in the equilibrium at room temperature; however, overemphasis on the precise quantitative population of the isomers in the $S_3^{n}Y_z^{\bullet}$ state would be undesirable because of the calculated small

https://doi.org/10.1021/jacs.2c03528
J. Am. Chem. Soc. 2022, 144, 11736−11747

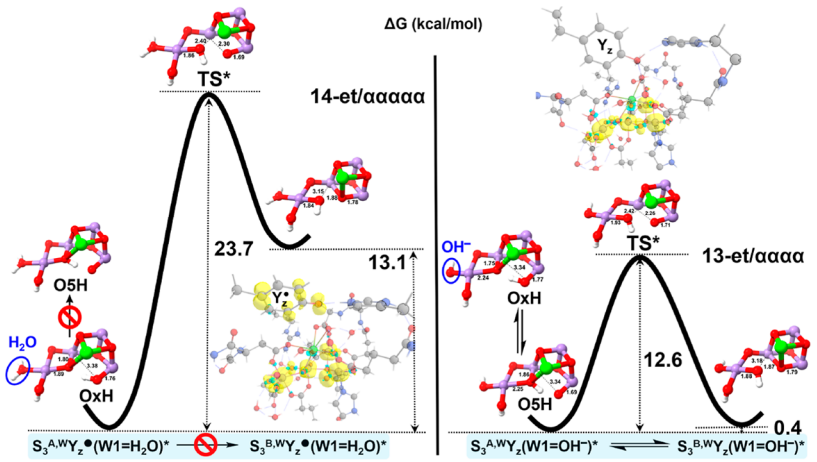

Figure 4. Relative Gibbs free energy profiles for the conversions between the virtual states $S_3^{A,W}Y_z^{\bullet}(W1{=}H_2O)^*$ and $S_3^{B,W}Y_z^{\bullet}(W1{=}H_2O)^*$ (left) and between the virtual states $S_3^{A,W}Y_z(W1{=}OH^-)^*$ and $S_3^{B,W}Y_z(W1{=}OH^-)^*$ (right) in their respective highest spin states; "*" denotes a virtual state.

energy gap and the well-known intrinsic limitations in the accuracy of DFT methodology,[97−100] and the ambiguous direction of the equilibrium shifting given the consumption of $S_3^{A,W}Y_z^{\bullet}$ and/or $S_3^{B,W}Y_z^{\bullet}$ when proceeding to the S_4 state. Thus, the isomerism suggested here in $S_3{}^nY_z^{\bullet}$ resembles the situations in the S_1 and S_2 states,[31,32,41] where the closed-cubane structures are also deemed important for the catalytic progression despite the calculated slight energetic disadvantages compared with the open-cubane forms, that is, +3.2 kcal/mol for S_1^B and +(1−2) kcal/mol for S_2^B (see Text S3 in the Supporting Information for the detailed analysis).[26,31,32,41,48,101−104] As a consequence of the markedly closer energies of the isomers in the $S_3{}^nY_z^{\bullet}$ state, the predominance of the open-cubane structure is undermined and the significance of $S_3^{B,W}Y_z^{\bullet}$ should be highlighted in addition to $S_3^{A,W}Y_z^{\bullet}$. Strictly speaking, one should not overlook the importance of either isomer in the $S_3{}^nY_z^{\bullet}$ state, considering the aforementioned uncertain factors that would lead to an indefinite identification of a dominant or most reactive component.

Besides the thermodynamics, the free energy barriers from $S_3^{A,W}Y_z^{\bullet}$ to $S_3^{B,W}Y_z^{\bullet}$ for all the possible spin states are dramatically reduced to 14.8−16.2 kcal/mol (vs 24.3−25.6 kcal/mol in the $S_3{}^+Y_z$ state), which allows for smooth production of $S_3^{B,W}Y_z^{\bullet}$ at a level of milliseconds kinetics (see Text S4 in the Supporting Information for more details). It is noteworthy that the direct reactant for the isomerization turns out to involve the protonated O5H, which is reachable by facile deprotonation from Ox and vice versa (Figure 3d); this remarkably contrasts the situation in the $S_3{}^+Y_z$ state, where O5H is not achievable for $S_3^{A,W}$ (Figure 2d). These results show a feasible pathway from $S_3^{A,W}Y_z^{\bullet}$ to $S_3^{B,W}Y_z^{\bullet}$ preceded by Ox deprotonation and demonstrate that the structural heterogeneity lost in the $S_3{}^+Y_z$ state becomes available again in the $S_3{}^nY_z^{\bullet}$ state. This leads to a more balanced constituent of the isomers, as compared to the dominance of the $S_3^{A,W}$ conformation and the high energetic barrier for isomerization in the $S_3{}^+Y_z$ state.

W1 Deprotonation Facilitates the Open-to-Closed Isomerization. As shown above, a magnitude of ca. 10 kcal/mol decrease in both barrier heights and relative energies from $S_3{}^+Y_z$ to $S_3{}^nY_z^{\bullet}$ has largely changed the equilibrium distribution of the isomers. This is mainly manifested in the feasibility of $S_3^{A,W}Y_z^{\bullet}$ converting to $S_3^{B,W}Y_z^{\bullet}$, since B to A is attainable in both the $S_3{}^+Y_z$ and $S_3{}^nY_z^{\bullet}$ states. Quite evidently, the $S_3{}^nY_z^{\bullet}(W1{=}OH^-)$ state is differentiated from $S_3{}^+Y_z(W1{=}H_2O)$ by its oxidized $Y_z^{\bullet}$ unit and deprotonated W1 ligand, that is, the asynchronous departure of an electron and a proton from two separated sites. Thus, two virtual states $S_3{}^+Y_z^{\bullet}(W1{=}H_2O)^*$ and $S_3{}^nY_z(W1{=}OH^-)^*$ characterizing the single effect were artificially fabricated in order to clarify the ultimate reason for the observed difference. Since the spin state selectivity is expected to bring little impact on the isomerization, only the highest spin states were studied for a comparison, as shown in Figure 4.

The situation for the virtual $S_3{}^+Y_z^{\bullet}(W1{=}H_2O)^*$ and $S_3{}^nY_z(W1{=}OH^-)^*$ states fairly coincides with that of the $S_3{}^+Y_z(W1{=}H_2O)$ and $S_3{}^nY_z^{\bullet}(W1{=}OH^-)$ states, respectively, in terms of the reaction energetics and geometric parameters (Tables S5−S8 in the Supporting Information), as well as the proton mobility between Ox and O5 (Figures S2 and S3 in the Supporting Information). The comparison clearly reveals that it is the occurrence of W1(H_2O) deprotonation, rather than appearance of the $Y_z^{\bullet}$ radical, that substantially promotes the A to B isomerization in the $S_3{}^nY_z^{\bullet}$ state. This is reasonable because the covalent bonding interactions within the Mn_4CaO_6 cluster should be much more powerful than the electrostatic effect brought by the distal $Y_z^{\bullet}$ group. Specifically, we expect that the strong σ donation from W1═OH^- reinforces its coordination to Mn4 but considerably weakens the O5−Mn4 bonding, due to the "structural trans effect" in octahedral transition metal complexes.[105−108] The diminished overlap between the Mn4 3d and O5 2p orbitals can in turn stabilize the O5 2p−H s covalency, increasing the basicity of O5 and explaining the accessibility of O5 protonation in both $S_3^{A,W}Y_z^{\bullet}(W1{=}OH^-)$ and $S_3^{A,W}Y_z(W1{=}OH^-)^*$. Furthermore, the Mn3−O5 bond is weakened by the protonated O5H, which therefore becomes easier to be substituted by Ox (oxo). The altered bond strengths can be seen from variations of the key bond lengths and Wiberg bond orders (Table S9 in the Supporting Information). To sum up, the feasibility of the open-to-closed isomerization in the $S_3{}^nY_z^{\bullet}$ state is directly attributable to W1(H_2O) deprotonation, which causes a series of subtle changes in Mn−ligand interactions.

Although $Y_z^{\bullet}$ itself produces little chemical effect on the isomerization, its formation is necessary for the subsequent

https://doi.org/10.1021/jacs.2c03528
J. Am. Chem. Soc. 2022, 144, 11736−11747

W1(H_2O) deprotonation. After the third flash given to dark-adapted PSII, the $S_3^+Y_z^\bullet$ state forms accompanied by deprotonation of the phenolic oxygen of Y_z to the ε-nitrogen of His190, and thus an extra positive charge accumulates within the vicinity of the Mn_4CaO_6 cluster. Thereafter, the Mn4-bound W1 serves as an ideal deprotonation site for charge compensation because it is in strong hydrogen-bonding interaction with the negatively charged D1-Asp61, which connects further to the proton exit channel and the lumen.[39,52,56,81,95,109−114] Thereby, the occurrence of Y_z oxidation is an essential prerequisite for the reversible structural isomerization in the $S_3Y_z^\bullet$ state, from a perspective of the causal relationship.

It is noted that up to date, there is still no unambiguous/conclusive assignment for the protonation states of the titrable groups (especially W2 and Ox) of the OEC cluster in the $S_3^+Y_z$ and $S_3{}^nY_z^\bullet$ states; however, our models adopt the protonation states suggested by Cox et al.,[57] which reproduced the experimental EPR and electron−nuclear double resonance (ENDOR) and electron−electron double resonance-detected nuclear magnetic resonance (EDNMR) of the S_3 state, and are in good agreement with most computational studies.[51,60,61,91,94,115−118] Still, we have also performed extensive additional computations and found that our conclusion still holds even if different protonation state distributions were considered (see Text S5 and Tables S10−S14 in the Supporting Information for the details).

Alternative Computational S_3 State Models. For the $S_3^+Y_z$ and $S_3{}^nY_z^\bullet$ states, Corry and O'Malley proposed "oxo−hydroxo ⇌ oxo−oxo ⇌ peroxo" and "oxo−oxo ⇌ peroxo" equilibria to describe the chemical nature of "O5−Ox" in $S_3^+Y_z$ and $S_3{}^nY_z^\bullet$, respectively.[65,67] Early O−O bond formation in the S_3 state was also explored by Pushkar et al.[64] and Isobe et al.[58,59] We note that the "oxo-hydroxo" model with all octahedral Mn(IV) employed in this study adequately fits the vast majority of results from EXAFS,[5,116,119,120] EPR/ENDOR/EDNMR, and X-ray absorption and emission spectroscopies in the S_3 state.[57,118,121] In contrast, while it still remains unclear if the "oxo−oxo" model is consistent with these spectroscopic data, the "peroxo" model would produce two anisotropic Mn(III) and thus is clearly inconsistent with the experimental observations. It has been also ruled out by all the latest XFEL experiments with updated essential details (e.g., O5−O6/Ox distance),[36−39] despite support from one initial study.[35] The calculated S = 4 ground state of the peroxo model[65] does not agree with the S = 3 signal observed experimentally.[57] On the basis of substrate-water exchange,[24,122] although we cannot fully exclude the "peroxo" model given the option of suitable structural/redox equilibria, obviously a stable peroxide can be ruled out. From the aspect of computational modeling, calculations by coupled cluster theory, which is beyond traditional DFT, also strongly disfavors the scenario based on an early-onset O−O bond formation in the S_3 state.[123]

However, it remains possible that the "peroxo" form could constitute part of the redox equilibria in the S_3 state and it might be catalytically relevant, but it should not represent the dominant form in the S_3 state. For the $S_3{}^nY_z^\bullet$ state, the "peroxo" model was indeed considered as one possible option because water exchange dramatically slows down as compared to S_3,[124] but the model was also ruled out by the authors in that report because of the inconsistency with the results from time-resolved X-ray experiments.[3,70,124] Still, we have in detail considered the "oxo−oxo" model in both the $S_3^+Y_z$ and $S_3{}^nY_z^\bullet$ states (Text S5 and Tables S12−S14 in the Supporting Information), and we can conclude that it does not change the basic conclusion of this study. Finally, we emphasize that the "oxo-hydroxo" model should be adopted (for cyanobacterial PSII) because of its representation of the most stable form of the ground state in the dominant population of the $S_3^+Y_z$ and its derived $S_3{}^nY_z^\bullet$ states; for high-plants, the "oxo-hydroxo" model is also valid in the novel closed-cubane S_3 structure according to Zahariou et al.,[68] but the circumstances of the structural isomerization, if exist in the water-unbound form, would need further investigations.

Comparison to Experimental Observations. Since experimental techniques probing into the $S_3 \rightarrow S_4$ transition remain difficult, so far there is very limited information regarding the morphological changes of the $Mn_4CaO_{5(6)}$ cluster upon formation of the $S_3{}^nY_z^\bullet$ state. Therefore, the structural isomerization found in this study should be seen as a theoretical prediction pending experimental verification. However, some suggestive evidence still exists in support of our proposal.

Nilsson et al. discovered that substrate-water exchange is arrested in the $S_3{}^nY_z^\bullet$ state because of the observed dramatically slowed kinetics as compared to earlier S states.[124] As discussed therein, the possible reasons include the impossibility to generate a Mn(III) center that is required for water exchange,[91] H^+ release that leads to much stronger binding of the deprotonated group, and reconstruction of the H-bonding network after proton-coupled electron transfer upon Y_z oxidation. Our proposed reversible isomerization is compatible with the observation because, in contrast to the $S_3{}^{A,W}Y_z \rightleftharpoons S_2Y_z^\bullet$ equilibrium that supports water exchange in the $S_3^+Y_z$ state, the $S_3{}^{A,W}Y_z^\bullet \rightleftharpoons S_3{}^{B,W}Y_z^\bullet$ equilibrium does not facilitate water exchange due to the lack of Mn(III) formation. In fact, the chemical equilibrium would cause extensive rearrangement of the locations and H-bonding orientations of water molecules and may thus even contribute to slowing down the rate of substrate water exchange in the $S_3{}^nY_z^\bullet$ state. Such changes in the H-bonding network have also been suggested to affect the distribution of the conformational microstates of water molecules and to thereby affect the rate of the $S_3{}^nY_z^\bullet \rightarrow S_0Y_z$ transition.[125]

Bao and Burnap studied the O_2 release kinetics by site-directed mutagenesis and found that both the lag and slow phases during the $S_3^+Y_z \rightarrow S_0{}^nY_z$ transition are retarded. On that basis, they suggested that "proton tautomerization" and/or "structural isomerization" precede(s) dioxygen formation.[93] Specifically, they suggested two interpretations. For proton tautomerization, they proposed that it would be followed by O−O bond formation via W3−W2 nucleophilic attack,[72,81,82,85] while in case of open-closed structural isomerization, O−O bond formation by oxo−oxyl radical coupling between W2 and O5 may occur, in line with previous suggestions.[80,83,84] We note that O−O bond formation via water nucleophilic attack (WNA) appears less favorable on the basis of recent experiments[36,37,124] and theoretical calculations.[71,126] Indeed, our present results provide further support for the variant radical coupling mechanism using a closed-cubane S_4 structure for O_2 evolution because our theoretical finding shows that the $S_4{}^{B,W}$ structure could be obtainable via the open-to-closed rearrangement in the $S_3{}^nY_z^\bullet$ state (rather than in the $S_3^+Y_z$ state as assumed in ref 84).

https://doi.org/10.1021/jacs.2c03528
J. Am. Chem. Soc. 2022, 144, 11736−11747

Scheme 2. Possible mechanisms of the $S_3 \rightarrow S_4$ transition and O−O Bond formation in the S_4 State[a]

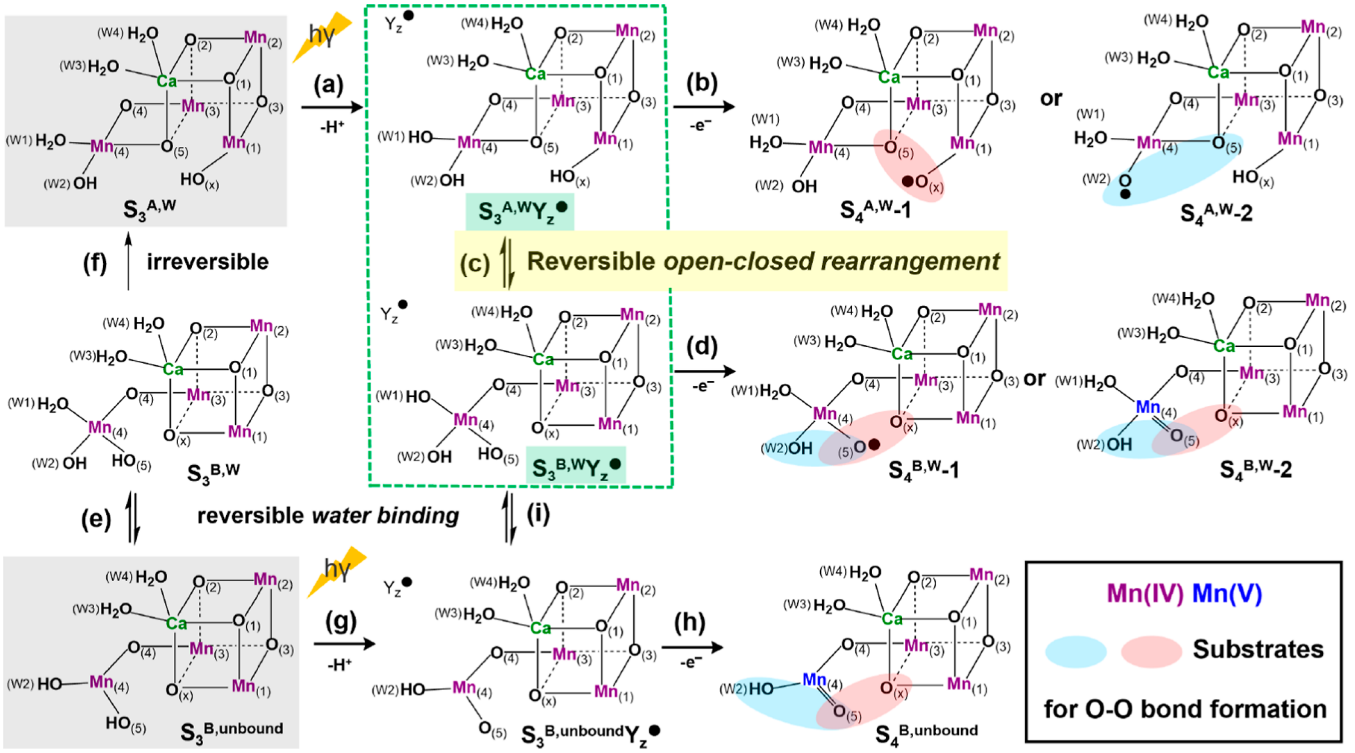

[a] $S_3^{A,W}$ and $S_3^{B,unbound}$ in gray stand for the two potential starting configurations in the S_3 state, resolved in cyanobacteria and higher-plant PSII by XFEL and EPR experiments, respectively.[35−38,44,68] The process focused in this work is highlighted in the green dashed box. Candidate substrates are encircled in red (favored) or blue (possible alternatives). Mn formal oxidation states (IV)(V) are displayed in different colors. The superscript "W"/"unbound" means hexa/penta-coordinate Mn4 with a water bound/unbound water trans to O5. The annotations for sequence numbers: (a,g) Y_z oxidation followed by proton release; (b,d,h) intramolecular proton transfer followed by Ox/W2/O5/Mn4 oxidation; (c) reversible open-closed rearrangement in the $S_3{}^nY_z^\bullet$ state, as proposed in this study; (e,i) reversible water binding to the five-coordinate Mn4(IV) in the closed-cubane structure; and (f) irreversible closed-to-open conversion in the S_3 state. Other proposed mechanisms are discussed in the text. It is noted that the oxygen labeling for $S_3^{B,W}$ and $S_3^{B,unbound}$ (and their derivatives) is chosen for consistency with that established by serial crystallography for the $S_3^{A,W}$[36,38,39] and for convenience to describe all the transitions uniformly. These labels do not reflect the origin of the oxygens with regard to the S_1 and S_2 states because several options for water insertion during the $S_2 \rightarrow S_3$ transition are still discussed;[6,7,32,38,43,48,52,62,82,101,120,132−139] an alternative nomenclature based on $S_3^{B,unbound}$ and the pivot/carousel water insertion is shown in Figure S4 in the Supporting Information.

Thus, the open-closed isomerization in the $S_3{}^nY_z^\bullet$ state may correspond to the proposed "structural isomerization" preceding dioxygen formation[93] and to thereby constitute the rate limiting 1−2 ms phase (slow phase) that follows a 200 μs lag phase (Figure 1d) and precedes the much more rapid O_2 formation.[3,12−22,92,127] According to the Eyring−Polanyi equation of TS theory assuming a standard pre-exponential factor,[128−130] the 1−2 ms kinetics is calculated to correspond to an activation free energy ∼14 kcal/mol at room temperature. Given the limited errors from DFT methodology and possibly experimental measurement, a safer quantity for the barrier should be around 13−15 kcal/mol for a process that occurs on a timescale of milliseconds.[71] Siegbahn ascribed the slow phase of O_2 formation to an intramolecular proton transfer step with 10.2 kcal/mol barrier,[52] but as he pointed out, considering a typical accuracy within 3−5 kcal/mol, which normally overestimates barriers for a DFT hybrid functional,[51,97,98,131] it is far below the required limit for a millisecond process.[52] By comparison, our calculated barriers of 14.8−16.2 kcal/mol for all the possible spin states are in much better agreement with the experimental kinetics (see Text S4 in the Supporting Information for more details). If the open-to-closed transition in the $S_3{}^nY_z^\bullet$ state was indeed the main rate limiting step for O_2 formation, this would mean that O_2 formation would start exclusively from the $S_3^{B,W}Y_z^\bullet$ state, and radical coupling from the $S_3^{A,W}Y_z^\bullet$ state would not be possible for reasons still to be determined. Thus, at the current stage of knowledge, we do not emphasize the proposed isomerization as the only possibility taking place in $S_3{}^nY_z^\bullet \rightarrow S_4{}^+Y_z$ before compelling experimental evidence emerges; however, the reversible open-to-closed structural rearrangement should be regarded as a viable mechanism or at least as part of processes responsible for the slow phase.

Implications for the Mechanism of O−O Bond Formation. The proposed reversible open-closed interconversion in the $S_3{}^nY_z^\bullet$ state has important implications for the mechanism of O−O bond formation in the S_4 state. This is illustrated in Scheme 2, which starts from the two structural architectures $S_3^{A,W}$ and $S_3^{B,unbound}$ observed by XFEL[35−38] and EPR experiments,[44,68] respectively. The first route (a) → (b) from $S_3^{A,W}$ to $S_4^{A,W}$-1 expresses Siegbahn's oxo(O5)−oxyl(Ox) coupling mechanism that he found to be energetically most favorable.[51,53,71,76] Here, the Mn1(IV)-bound Ox radical couples with μ-O5 in an open-cubane structure. Alternatively, the radical could be localized at W2 if it is deprotonated instead of Ox, and its coupling with μ-O5 in $S_4^{A,W}$-2 might be an option, which, however, has not gained support from recent DFT calculations.[79,84]

https://doi.org/10.1021/jacs.2c03528
J. Am. Chem. Soc. 2022, 144, 11736−11747

For the intermediate $S_3^{A,W}Y_z^{\bullet}$ state prior to S_4, our present results provide the first theoretical basis for the (reversible) conversion to $S_3^{B,W}Y_z^{\bullet}$ by route (c), thereby diversifying alternative pathways leading to O−O bond formation in the S_4 state with a closed-cubane type. Specifically, $S_3^{B,W}Y_z^{\bullet}$ with the octahedral Mn4(IV) coordination may proceed to S_4 by O5 or Mn4 oxidation through route (d), producing the O5 radical in $S_4^{B,W}$-1, or alternatively, Mn4(V) in $S_4^{B,W}$-2. Both options, W2−O5 coupling (blue) on Mn4 and O5−Ox coupling involving multiple metal (Mn and Ca) centers (red), are worth considering. It is noted that O5−Ox coupling in the $S_4^{B,W}$-1 state resembles the variant oxyl−oxo mechanism by Li and Siegbahn,[84] which was based on previous experimental proposals.[4,80,124]

The $S_3^{B,unbound}$ state may either evolve to $S_3^{A,W}$ via $S_3^{B,W}$ after (reversible) water binding by the "pivot" or "carousel" mechanism[43,44,120,132−134] through the route (e) → (f) and then advance to the O_2 formation routes described above, or, as suggested by Pantazis and collaborators, directly proceed to $S_4^{B,unbound}$ without water binding by the route (g) → (h).[68,69,87] The latter pathway involves a penta-coordinate Mn4(IV) center and would lead to Mn4(V) where nucleophilic Ox-O5 coupling[68,69,87] or hydroxo-oxo coupling between W2 and O5 might be possible. We note that the finding in the present study can provide an additional route (a) → (c) → (i) → (h) from $S_3^{A,W}$ to $S_4^{B,unbound}$ (other than from $S_3^{B,unbound}$).

Alternative mechanisms proposed in the literature include WNA from Ca-bound W3 onto the electron-deficient Mn4(V)=O (W2)[6,72,81,85] and oxyl-oxo coupling between W1 and μ-oxo O4.[78] Both appear inconsistent with mass spectrometric and EPR-based substrate water exchange data, which show that both substrates are bound to Mn(IV) in the $S_3^{+}Y_z$ and $S_3Y_z^{\bullet}$ states (excluding WNA),[122,124] and are best consistent with O5 as the slow exchanging substrate water.[4,24,80,83,122,124,140−143] Nevertheless, these suggestions will also be further scrutinized in future DFT calculations.

Since $S_3^{A,W}Y_z^{\bullet}$ and $S_3^{B,W}Y_z^{\bullet}$ are nearly isoenergetic and for both states, low-energy routes for O−O bond formation via radical coupling have been determined,[51,84] the intriguing possibility arises from the results of this study that O−O bond formation may occur via two routes, or even more, if also the $S_3^{B,unbound}Y_z^{\bullet} \rightarrow S_4^{B,unbound}Y_z \rightarrow S_0Y_z$ path in "water-deficient" catalytic sites is taken into account.[68,69] While recent water exchange experiments in the S_2 state have reported first evidence for two possible fast exchanging water substrates,[24,122] the current water exchange data in the S_3 state are best consistent with only one set of substrate waters. This would favor that either $S_4^{B,W}/S_4^{B,unbound}$ (substrates: W2 and O5) or $S_4^{A,W}$ (substrates: Ox and O5) would be involved. However, the present study suggests that the energetic and kinetic differences between these possible routes are so small that minor differences between species or experimental conditions could favor one or the other pathway.

CONCLUSIONS

In summary, we have identified a reversible open-to-closed isomerization for the $S_3^{n}Y_z^{\bullet}$ state, in contrast to the unidirectional conversion in the $S_3^{+}Y_z$ state. This isomerization immediately before O_2 formation is activated by deprotonation of a Mn-bound water (W1) after tyrosine Y_z oxidation. The structural rearrangement may constitute or contribute to the slow kinetic phase that prepares the Mn_4CaO_6 cluster for O_2 formation. Thus, the restored structural heterogeneity prior to the S_4 state diversifies the viable options for O−O bond formation in PSII. In this way, the availability of both open and closed-cubane structures in the S_4 state may reflect a "two-pronged" arrangement of the OEC, allowing for efficient and robust water oxidation, and may have contributed to its evolutionary development. The elegant structural reversibility triggered by proton release in the natural enzyme may provide a useful reference for designs of artificial catalysts.

ASSOCIATED CONTENT

Supporting Information

The Supporting Information is available free of charge at https://pubs.acs.org/doi/10.1021/jacs.2c03528.

Model construction, spin state definition, computational details, supplementary texts, tables, figures, and references, and optimized Cartesian coordinates (PDF)

AUTHOR INFORMATION

Corresponding Authors

Johannes Messinger − *Department of Chemistry, Umeå University, SE-90187 Umeå, Sweden; Molecular Biomimetics, Department of Chemistry—Ångström Laboratory, Uppsala University, SE-75120 Uppsala, Sweden;* orcid.org/0000-0003-2790-7721; Email: johannes.messinger@kemi.uu.se

Lars Kloo − *Department of Chemistry, School of Engineering Sciences in Chemistry, Biotechnology and Health, KTH Royal Institute of Technology, SE-10044 Stockholm, Sweden;* orcid.org/0000-0002-0168-2942; Email: larsa@kth.se

Licheng Sun − *Center of Artificial Photosynthesis for Solar Fuels and Department of Chemistry, School of Science, Westlake University, Hangzhou 310024, China; Institute of Natural Sciences, Westlake Institute for Advanced Study, Hangzhou 310024, China;* orcid.org/0000-0002-4521-2870; Email: sunlicheng@westlake.edu.cn

Author

Yu Guo − *Center of Artificial Photosynthesis for Solar Fuels and Department of Chemistry, School of Science, Westlake University, Hangzhou 310024, China; Institute of Natural Sciences, Westlake Institute for Advanced Study, Hangzhou 310024, China*

Complete contact information is available at: https://pubs.acs.org/10.1021/jacs.2c03528

Notes

The authors declare no competing financial interest.

ACKNOWLEDGMENTS

This work is financially supported by the starting-up package of Westlake University (to L.S.), the Swedish Research Council 2020-03809 (to J.M.) and 2020-06701 (to L.K.). We thank Westlake University HPC Center for computation support.

REFERENCES

(1) Messinger, J.; Renger, G. Photosynthetic water splitting. *Primary Processes of Photosynthesis, Part 2: Principles and Apparatus*; The Royal Society of Chemistry, 2008; Vol. 9, pp 291−349.

(2) Barber, J. Photosynthetic energy conversion: natural and artificial. *Chem. Soc. Rev.* **2009**, *38*, 185−196.

(3) Dau, H.; Zaharieva, I.; Haumann, M. Recent developments in research on water oxidation by photosystem II. *Curr. Opin. Chem. Biol.* **2012**, *16*, 3−10.

(4) Cox, N.; Messinger, J. Reflections on substrate water and dioxygen formation. *Biochim. Biophys. Acta, Bioenerg.* **2013**, *1827*, 1020−1030.
(5) Yano, J.; Yachandra, V. Mn_4Ca cluster in photosynthesis: where and how water is oxidized to dioxygen. *Chem. Rev.* **2014**, *114*, 4175−4205.
(6) Vinyard, D. J.; Brudvig, G. W. Progress toward a molecular mechanism of water oxidation in photosystem II. *Annu. Rev. Phys. Chem.* **2017**, *68*, 101−116.
(7) Pantazis, D. A. Missing pieces in the puzzle of biological water oxidation. *ACS Catal.* **2018**, *8*, 9477−9507.
(8) Lubitz, W.; Chrysina, M.; Cox, N. Water oxidation in photosystem II. *Photosynth. Res.* **2019**, *142*, 105−125.
(9) Junge, W. Oxygenic photosynthesis: history, status and perspective. *Q. Rev. Biophys.* **2019**, *52*, No. e1.
(10) Cox, N.; Pantazis, D. A.; Lubitz, W. Current understanding of the mechanism of water oxidation in photosystem II and its relation to XFEL data. *Annu. Rev. Biochem.* **2020**, *89*, 795−820.
(11) Kok, B.; Forbush, B.; McGloin, M. Cooperation of charges in photosynthetic O_2 evolution. I. a linear four-step mechanism. *Photochem. Photobiol.* **1970**, *11*, 457−475.
(12) Rappaport, F.; Blanchard-Desce, M.; Lavergne, J. Kinetics of electron transfer and electrochromic change during the redox transitions of the photosynthetic oxygen-evolving complex. *Biochim. Biophys. Acta, Bioenerg.* **1994**, *1184*, 178−192.
(13) Dau, H.; Haumann, M. Eight steps preceding O-O bond formation in oxygenic photosynthesis-A basic reaction cycle of the photosystem II manganese complex. *Biochim. Biophys. Acta, Bioenerg.* **2007**, *1767*, 472−483.
(14) Dau, H.; Haumann, M. Time-resolved X-ray spectroscopy leads to an extension of the classical S-state cycle model of photosynthetic oxygen evolution. *Photosynth. Res.* **2007**, *92*, 327−343.
(15) Klauss, A.; Haumann, M.; Dau, H. Alternating electron and proton transfer steps in photosynthetic water oxidation. *Proc. Natl. Acad. Sci. U.S.A.* **2012**, *109*, 16035−16040.
(16) Kato, Y.; Shibamoto, T.; Yamamoto, S.; Watanabe, T.; Ishida, N.; Sugiura, M.; Rappaport, F.; Boussac, A. Influence of the PsbA1/PsbA3, Ca^{2+}/Sr^{2+} and Cl^-/Br^- exchanges on the redox potential of the primary quinone Q_A in photosystem II from Thermosynechococcus elongatus as revealed by spectroelectrochemistry. *Biochim. Biophys. Acta, Bioenerg.* **2012**, *1817*, 1998−2004.
(17) Klauss, A.; Haumann, M.; Dau, H. Seven steps of alternating electron and proton transfer in photosystem II water oxidation traced by time-resolved photothermal beam deflection at improved sensitivity. *J. Phys. Chem. B* **2014**, *119*, 2677−2689.
(18) Boussac, A.; Rutherford, A. W.; Sugiura, M. Electron transfer pathways from the S_2-states to the S_3-states either after a Ca^{2+}/Sr^{2+}or a Cl^-/I^- exchange in photosystem II from Thermosynechococcus elongatus. *Biochim. Biophys. Acta, Bioenerg.* **2015**, *1847*, 576−586.
(19) Noguchi, T. Fourier transform infrared difference and time-resolved infrared detection of the electron and proton transfer dynamics in photosynthetic water oxidation. *Biochim. Biophys. Acta, Bioenerg.* **2015**, *1847*, 35−45.
(20) Debus, R. J. FTIR studies of metal ligands, networks of hydrogen bonds, and water molecules near the active site Mn_4CaO_5 cluster in photosystem II. *Biochim. Biophys. Acta, Bioenerg.* **2015**, *1847*, 19−34.
(21) Zaharieva, I.; Dau, H. Energetics and kinetics of S-State transitions monitored by delayed chlorophyll fluorescence. *Front. Plant Sci.* **2019**, *10*, 386.
(22) Mäusle, S. M.; Abzaliyeva, A.; Greife, P.; Simon, P. S.; Perez, R.; Zilliges, Y.; Dau, H. Activation energies for two steps in the $S_2 \rightarrow S_3$ transition of photosynthetic water oxidation from time-resolved single-frequency infrared spectroscopy. *J. Chem. Phys.* **2020**, *153*, 215101.
(23) Renger, G. Mechanism of light induced water splitting in photosystem II of oxygen evolving photosynthetic organisms. *Biochim. Biophys. Acta, Bioenerg.* **2012**, *1817*, 1164−1176.
(24) de Lichtenberg, C.; Messinger, J. Substrate water exchange in the S_2 state of photosystem II is dependent on the conformation of the Mn_4Ca cluster. *Phys. Chem. Chem. Phys.* **2020**, *22*, 12894−12908.
(25) Dismukes, G. C.; Siderer, Y. Intermediates of a polynuclear manganese center involved in photosynthetic oxidation of water. *Proc. Natl. Acad. Sci. U.S.A.* **1981**, *78*, 274−278.
(26) Boussac, A.; Ugur, I.; Marion, A.; Sugiura, M.; Kaila, V. R. I.; Rutherford, A. W. The low spin-high spin equilibrium in the S_2-state of the water oxidizing enzyme. *Biochim. Biophys. Acta, Bioenerg.* **2018**, *1859*, 342−356.
(27) Boussac, A.; Rutherford, A. W. Comparative study of the g=4.1 EPR signals in the S_2 state of photosystem II. *Biochim. Biophys. Acta, Bioenerg.* **2000**, *1457*, 145−156.
(28) Pokhrel, R.; Brudvig, G. W. Oxygen-evolving complex of photosystem II: correlating structure with spectroscopy. *Phys. Chem. Chem. Phys.* **2014**, *16*, 11812−11821.
(29) Zimmermann, J. L.; Rutherford, A. W. EPR studies of the oxygen-evolving enzyme of Photosystem II. *Biochim. Biophys. Acta, Bioenerg.* **1984**, *767*, 160−167.
(30) Casey, J. L.; Sauer, K. EPR detection of a cryogenically photogenerated intermediate in photosynthetic oxygen evolution. *Biochim. Biophys. Acta, Bioenerg.* **1984**, *767*, 21−28.
(31) Pantazis, D. A.; Ames, W.; Cox, N.; Lubitz, W.; Neese, F. Two interconvertible structures that explain the spectroscopic properties of the oxygen-evolving complex of photosystem II in the S_2 state. *Angew. Chem., Int. Ed.* **2012**, *51*, 9935−9940.
(32) Bovi, D.; Narzi, D.; Guidoni, L. The S_2 state of the oxygen-evolving complex of photosystem II explored by QM/MM dynamics: spin surfaces and metastable states suggest a reaction path towards the S_3 state. *Angew. Chem., Int. Ed.* **2013**, *52*, 11744−11749.
(33) Umena, Y.; Kawakami, K.; Shen, J.-R.; Kamiya, N. Crystal structure of oxygen-evolving photosystem II at a resolution of 1.9 Å. *Nature* **2011**, *473*, 55−60.
(34) Suga, M.; Akita, F.; Hirata, K.; Ueno, G.; Murakami, H.; Nakajima, Y.; Shimizu, T.; Yamashita, K.; Yamamoto, M.; Ago, H.; Shen, J.-R. Native structure of photosystem II at 1.95 Å resolution viewed by femtosecond X-ray pulses. *Nature* **2015**, *517*, 99−103.
(35) Suga, M.; Akita, F.; Sugahara, M.; Kubo, M.; Nakajima, Y.; Nakane, T.; Yamashita, K.; Umena, Y.; Nakabayashi, M.; Yamane, T.; Nakano, T.; Suzuki, M.; Masuda, T.; Inoue, S.; Kimura, T.; Nomura, T.; Yonekura, S.; Yu, L.-J.; Sakamoto, T.; Motomura, T.; Chen, J.-H.; Kato, Y.; Noguchi, T.; Tono, K.; Joti, Y.; Kameshima, T.; Hatsui, T.; Nango, E.; Tanaka, R.; Naitow, H.; Matsuura, Y.; Yamashita, A.; Yamamoto, M.; Nureki, O.; Yabashi, M.; Ishikawa, T.; Iwata, S.; Shen, J.-R. Light-induced structural changes and the site of O=O bond formation in PSII caught by XFEL. *Nature* **2017**, *543*, 131−135.
(36) Kern, J.; Chatterjee, R.; Young, I. D.; Fuller, F. D.; Lassalle, L.; Ibrahim, M.; Gul, S.; Fransson, T.; Brewster, A. S.; Alonso-Mori, R.; Hussein, R.; Zhang, M.; Douthit, L.; de Lichtenberg, C.; Cheah, M. H.; Shevela, D.; Wersig, J.; Seuffert, I.; Sokaras, D.; Pastor, E.; Weninger, C.; Kroll, T.; Sierra, R. G.; Aller, P.; Butryn, A.; Orville, A. M.; Liang, M.; Batyuk, A.; Koglin, J. E.; Carbajo, S.; Boutet, S.; Moriarty, N. W.; Holton, J. M.; Dobbek, H.; Adams, P. D.; Bergmann, U.; Sauter, N. K.; Zouni, A.; Messinger, J.; Yano, J.; Yachandra, V. K. Structures of the intermediates of Kok's photosynthetic water oxidation clock. *Nature* **2018**, *563*, 421−425.
(37) Suga, M.; Akita, F.; Yamashita, K.; Nakajima, Y.; Ueno, G.; Li, H.; Yamane, T.; Hirata, K.; Umena, Y.; Yonekura, S.; Yu, L.-J.; Murakami, H.; Nomura, T.; Kimura, T.; Kubo, M.; Baba, S.; Kumasaka, T.; Tono, K.; Yabashi, M.; Isobe, H.; Yamaguchi, K.; Yamamoto, M.; Ago, H.; Shen, J.-R. An oxyl/oxo mechanism for oxygen-oxygen coupling in PSII revealed by an x-ray free-electron laser. *Science* **2019**, *366*, 334−338.
(38) Ibrahim, M.; Fransson, T.; Chatterjee, R.; Cheah, M. H.; Hussein, R.; Lassalle, L.; Sutherlin, K. D.; Young, I. D.; Fuller, F. D.; Gul, S.; Kim, I.-S.; Simon, P. S.; de Lichtenberg, C.; Chernev, P.; Bogacz, I.; Pham, C. C.; Orville, A. M.; Saichek, N.; Northen, T.; Batyuk, A.; Carbajo, S.; Alonso-Mori, R.; Tono, K.; Owada, S.; Bhowmick, A.; Bolotovsky, R.; Mendez, D.; Moriarty, N. W.; Holton,

J. M.; Dobbek, H.; Brewster, A. S.; Adams, P. D.; Sauter, N. K.; Bergmann, U.; Zouni, A.; Messinger, J.; Kern, J.; Yachandra, V. K.; Yano, J. Untangling the sequence of events during the $S_2 \rightarrow S_3$ transition in photosystem II and implications for the water oxidation mechanism. *Proc. Natl. Acad. Sci. U.S.A.* **2020**, *117*, 12624−12635.
(39) Hussein, R.; Ibrahim, M.; Bhowmick, A.; Simon, P. S.; Chatterjee, R.; Lassalle, L.; Doyle, M.; Bogacz, I.; Kim, I.-S.; Cheah, M. H.; Gul, S.; de Lichtenberg, C.; Chernev, P.; Pham, C. C.; Young, I. D.; Carbajo, S.; Fuller, F. D.; Alonso-Mori, R.; Batyuk, A.; Sutherlin, K. D.; Brewster, A. S.; Bolotovsky, R.; Mendez, D.; Holton, J. M.; Moriarty, N. W.; Adams, P. D.; Bergmann, U.; Sauter, N. K.; Dobbek, H.; Messinger, J.; Zouni, A.; Kern, J.; Yachandra, V. K.; Yano, J. Structural dynamics in the water and proton channels of photosystem II during the S_2 to S_3 transition. *Nat. Commun.* **2021**, *12*, 6531.
(40) Chatterjee, R.; Lassalle, L.; Gul, S.; Fuller, F. D.; Young, I. D.; Ibrahim, M.; de Lichtenberg, C.; Cheah, M. H.; Zouni, A.; Messinger, J.; Yachandra, V. K.; Kern, J.; Yano, J. Structural isomers of the S_2 state in photosystem II: do they exist at room temperature and are they important for function? *Physiol. Plant.* **2019**, *166*, 60−72.
(41) Drosou, M.; Zahariou, G.; Pantazis, D. A. Orientational Jahn-Teller isomerism in the dark-stable state of nature's water oxidase. *Angew. Chem., Int. Ed.* **2021**, *60*, 13493−13499.
(42) Retegan, M.; Pantazis, D. A. Differences in the active site of water oxidation among photosynthetic organisms. *J. Am. Chem. Soc.* **2017**, *139*, 14340−14343.
(43) Retegan, M.; Krewald, V.; Mamedov, F.; Neese, F.; Lubitz, W.; Cox, N.; Pantazis, D. A. A five-coordinate Mn(IV) intermediate in biological water oxidation: spectroscopic signature and a pivot mechanism for water binding. *Chem. Sci.* **2016**, *7*, 72−84.
(44) Chrysina, M.; Heyno, E.; Kutin, Y.; Reus, M.; Nilsson, H.; Nowaczyk, M. M.; DeBeer, S.; Neese, F.; Messinger, J.; Lubitz, W.; Cox, N. Five-coordinate Mn^{IV} intermediate in the activation of nature's water splitting cofactor. *Proc. Natl. Acad. Sci. U.S.A.* **2019**, *116*, 16841−16846.
(45) Narzi, D.; Bovi, D.; Guidoni, L. Pathway for Mn-cluster oxidation by tyrosine-Z in the S_2 state of photosystem II. *Proc. Natl. Acad. Sci. U.S.A.* **2014**, *111*, 8723−8728.
(46) Corry, T. A.; O'Malley, P. J. Proton isomers rationalize the high- and low-spin forms of the S_2 state intermediate in the water-oxidizing reaction of photosystem II. *J. Phys. Chem. Lett.* **2019**, *10*, 5226−5230.
(47) Corry, T. A.; O'Malley, P. J. Molecular identification of a high-spin deprotonated intermediate during the S_2 to S_3 transition of nature's water-oxidizing complex. *J. Am. Chem. Soc.* **2020**, *142*, 10240−10243.
(48) Siegbahn, P. E. M. The S_2 to S_3 transition for water oxidation in PSII (photosystem II), revisited. *Phys. Chem. Chem. Phys.* **2018**, *20*, 22926−22931.
(49) Pushkar, Y.; Ravari, A. K.; Jensen, S. C.; Palenik, M. Early binding of substrate oxygen is responsible for a spectroscopically distinct S_2 state in photosystem II. *J. Phys. Chem. Lett.* **2019**, *10*, 5284−5291.
(50) Siegbahn, P. E. M. A structure-consistent mechanism for dioxygen formation in photosystem II. *Chem.—Eur. J.* **2008**, *14*, 8290−8302.
(51) Siegbahn, P. E. M. Structures and energetics for O_2 formation in photosystem II. *Acc. Chem. Res.* **2009**, *42*, 1871−1880.
(52) Siegbahn, P. E. M. Mechanisms for proton release during water oxidation in the S_2 to S_3 and S_3 to S_4 transitions in photosystem II. *Phys. Chem. Chem. Phys.* **2012**, *14*, 4849−4856.
(53) Siegbahn, P. E. M. Water oxidation mechanism in photosystem II, including oxidations, proton release pathways, O-O bond formation and O_2 release. *Biochim. Biophys. Acta, Bioenerg.* **2013**, *1827*, 1003−1019.
(54) Dau, H.; Andrews, J. C.; Roelofs, T. A.; Latimer, M. J.; Liang, W.; Yachandra, V. K.; Sauer, K.; Klein, M. P. Structural consequences of ammonia binding to the manganese center of the photosynthetic oxygen-evolving complex: an X-ray absorption spectroscopy study of isotropic and oriented photosystem II particles. *Biochemistry* **1995**, *34*, 5274−5287.
(55) Haumann, M.; Müller, C.; Liebisch, P.; Iuzzolino, L.; Dittmer, J.; Grabolle, M.; Neisius, T.; Meyer-Klaucke, W.; Dau, H. Structural and oxidation state changes of the photosystem II manganese complex in four transitions of the water oxidation cycle ($S_0 \rightarrow S_1$, $S_1 \rightarrow S_2$, $S_2 \rightarrow S_3$, and $S_{3,4} \rightarrow S_0$) characterized by X-ray absorption spectroscopy at 20 K and room temperature. *Biochemistry* **2005**, *44*, 1894−1908.
(56) Dau, H.; Haumann, M. The manganese complex of photosystem II in its reaction cycle-Basic framework and possible realization at the atomic level. *Coord. Chem. Rev.* **2008**, *252*, 273−295.
(57) Cox, N.; Retegan, M.; Neese, F.; Pantazis, D. A.; Boussac, A.; Lubitz, W. Electronic structure of the oxygen-evolving complex in photosystem II prior to O-O bond formation. *Science* **2014**, *345*, 804−808.
(58) Isobe, H.; Shoji, M.; Shen, J.-R.; Yamaguchi, K. Chemical equilibrium models for the S_3 state of the oxygen-evolving complex of photosystem II. *Inorg. Chem.* **2016**, *55*, 502−511.
(59) Isobe, H.; Shoji, M.; Suzuki, T.; Shen, J.-R.; Yamaguchi, K. Spin, valence, and structural isomerism in the S_3 State of the oxygen-evolving complex of photosystem II as a manifestation of multi-metallic cooperativity. *J. Chem. Theory Comput.* **2019**, *15*, 2375−2391.
(60) Isobe, H.; Shoji, M.; Suzuki, T.; Shen, J.-R.; Yamaguchi, K. Exploring reaction pathways for the structural rearrangements of the Mn cluster induced by water binding in the S_3 state of the oxygen evolving complex of photosystem II. *J. Photochem. Photobiol., A* **2021**, *405*, 112905.
(61) Capone, M.; Bovi, D.; Narzi, D.; Guidoni, L. Reorganization of substrate waters between the closed and open cubane conformers during the S_2 to S_3 transition in the oxygen evolving complex. *Biochemistry* **2015**, *54*, 6439−6442.
(62) Shoji, M.; Isobe, H.; Yamaguchi, K. QM/MM study of the S_2 to S_3 transition reaction in the oxygen-evolving complex of photosystem II. *Chem. Phys. Lett.* **2015**, *636*, 172−179.
(63) Askerka, M.; Brudvig, G. W.; Batista, V. S. The O_2-evolving complex of photosystem II: recent insights from quantum mechanics/molecular mechanics (QM/MM), extended X-ray absorption fine structure (EXAFS), and femtosecond X-ray crystallography data. *Acc. Chem. Res.* **2017**, *50*, 41−48.
(64) Pushkar, Y.; Davis, K. M.; Palenik, M. C. Model of the oxygen evolving complex which is highly predisposed to O-O bond formation. *J. Phys. Chem. Lett.* **2018**, *9*, 3525−3531.
(65) Corry, T. A.; O'Malley, P. J. Evidence of O-O bond formation in the final metastable S_3 state of nature's water oxidizing complex implying a novel mechanism of water oxidation. *J. Phys. Chem. Lett.* **2018**, *9*, 6269−6274.
(66) Corry, T. A.; O'Malley, P. J. Electronic−level View of O−O bond formation in nature's water oxidizing complex. *J. Phys. Chem. Lett.* **2020**, *11*, 4221−4225.
(67) Corry, T. A.; O'Malley, P. J. S_3 state models of nature's water oxidizing complex: analysis of bonding and magnetic exchange pathways, assessment of experimental electron paramagnetic resonance data, and Implications for the water oxidation mechanism. *J. Phys. Chem. B* **2021**, *125*, 10097−10107.
(68) Zahariou, G.; Ioannidis, N.; Sanakis, Y.; Pantazis, D. A. Arrested substrate binding resolves catalytic intermediates in higher-plant water oxidation. *Angew. Chem., Int. Ed.* **2021**, *60*, 3156−3162.
(69) Krewald, V.; Neese, F.; Pantazis, D. A. Implications of structural heterogeneity for the electronic structure of the final oxygen-evolving intermediate in photosystem II. *J. Inorg. Biochem.* **2019**, *199*, 110797.
(70) Haumann, M.; Liebisch, P.; Müller, C.; Barra, M.; Grabolle, M.; Dau, H. Photosynthetic O_2 formation tracked by time-resolved X-ray experiments. *Science* **2005**, *310*, 1019−1021.
(71) Siegbahn, P. E. M. O-O bond formation in the S_4 state of the oxygen-evolving complex in photosystem II. *Chem.—Eur. J.* **2006**, *12*, 9217−9227.

https://doi.org/10.1021/jacs.2c03528
J. Am. Chem. Soc. 2022, 144, 11736−11747

(72) Vinyard, D. J.; Khan, S.; Brudvig, G. W. Photosynthetic water oxidation: binding and activation of substrate waters for O-O bond formation. *Faraday Discuss.* **2015**, *185*, 37−50.
(73) Shen, J.-R. The structure of photosystem II and the mechanism of water oxidation in photosynthesis. *Annu. Rev. Plant Biol.* **2015**, *66*, 23−48.
(74) Krewald, V.; Retegan, M.; Neese, F.; Lubitz, W.; Pantazis, D. A.; Cox, N. Spin state as a marker for the structural evolution of nature's water-splitting catalyst. *Inorg. Chem.* **2016**, *55*, 488−501.
(75) Guo, Y.; He, L.-L.; Zhao, D.-X.; Gong, L.-D.; Liu, C.; Yang, Z.-Z. How does ammonia bind to the oxygen-evolving complex in the S_2 state of photosynthetic water oxidation? Theoretical support and implications for the W1 substitution mechanism. *Phys. Chem. Chem. Phys.* **2016**, *18*, 31551−31565.
(76) Guo, Y.; Li, H.; He, L.-L.; Zhao, D.-X.; Gong, L.-D.; Yang, Z.-Z. The open-cubane oxo-oxyl coupling mechanism dominates photosynthetic oxygen evolution: a comprehensive DFT investigation on O-O bond formation in the S_4 state. *Phys. Chem. Chem. Phys.* **2017**, *19*, 13909−13923.
(77) Guo, Y.; Li, H.; He, L.-L.; Zhao, D.-X.; Gong, L.-D.; Yang, Z.-Z. Theoretical reflections on the structural polymorphism of the oxygen-evolving complex in the S_2 state and the correlations to substrate water exchange and water oxidation mechanism in photosynthesis. *Biochim. Biophys. Acta, Bioenerg.* **2017**, *1858*, 833−846.
(78) Kawashima, K.; Takaoka, T.; Kimura, H.; Saito, K.; Ishikita, H. O_2 evolution and recovery of the water-oxidizing enzyme. *Nat. Commun.* **2018**, *9*, 1247.
(79) Guo, Y.; Zhang, B.; Kloo, L.; Sun, L. Necessity of structural rearrangements for O-O bond formation between O5 and W2 in photosystem II. *J. Energy Chem.* **2021**, *57*, 436−442.
(80) Messinger, J. Evaluation of different mechanistic proposals for water oxidation in photosynthesis on the basis of Mn_4O_xCa structures for the catalytic site and spectroscopic data. *Phys. Chem. Chem. Phys.* **2004**, *6*, 4764−4771.
(81) Ferreira, K. N.; Iverson, T. M.; Maghlaoui, K.; Barber, J.; Iwata, S. Architecture of the photosynthetic oxygen-evolving center. *Science* **2004**, *303*, 1831−1838.
(82) Sproviero, E. M.; Gascón, J. A.; McEvoy, J. P.; Brudvig, G. W.; Batista, V. S. Quantum mechanics/molecular mechanics study of the catalytic cycle of water splitting in photosystem II. *J. Am. Chem. Soc.* **2008**, *130*, 3428−3442.
(83) Nilsson, H.; Krupnik, T.; Kargul, J.; Messinger, J. Substrate water exchange in photosystem II core complexes of the extremophilic red alga cyanidioschyzon merolae. *Biochim. Biophys. Acta, Bioenerg.* **2014**, *1837*, 1257−1262.
(84) Li, X.; Siegbahn, P. E. M. Alternative mechanisms for O_2 release and O-O bond formation in the oxygen evolving complex of photosystem II. *Phys. Chem. Chem. Phys.* **2015**, *17*, 12168−12174.
(85) Barber, J. A mechanism for water splitting and oxygen production in photosynthesis. *Nat. Plants* **2017**, *3*, 17041.
(86) Zhang, B.; Sun, L. Why nature chose the Mn_4CaO_5 cluster as water-splitting catalyst in photosystem II: a new hypothesis for the mechanism of O-O bond formation. *Dalton Trans.* **2018**, *47*, 14381−14387.
(87) Orio, M.; Pantazis, D. A. Successes, challenges, and opportunities for quantum chemistry in understanding metalloenzymes for solar fuels research. *Chem. Commun.* **2021**, *57*, 3952−3974.
(88) Vos, M. H.; van Gorkom, H. J.; van Leeuwen, P. J. An electroluminescence study of stabilization reactions in the oxygen-evolving complex of photosystem II. *Biochim. Biophys. Acta, Bioenerg.* **1991**, *1056*, 27−39.
(89) de Wijn, R.; van Gorkom, H. J. S-state dependence of the miss probability in photosystem II. *Photosynth. Res.* **2002**, *72*, 217−222.
(90) Geijer, P.; Morvaridi, F.; Styring, S. The S_3 state of the oxygen-evolving complex in photosystem II Is converted to the $S_2Y_Z\bullet$ state at alkaline pH. *Biochemistry* **2001**, *40*, 10881−10891.
(91) Siegbahn, P. E. M. Substrate water exchange for the oxygen evolving complex in PSII in the S_1, S_2, and S_3 states. *J. Am. Chem. Soc.* **2013**, *135*, 9442−9449.
(92) Razeghifard, M. R.; Pace, R. J. EPR kinetic studies of oxygen release in Thylakoids and PSII membranes: a kinetic intermediate in the S_3 to S_0 transition. *Biochemistry* **1999**, *38*, 1252−1257.
(93) Bao, H.; Burnap, R. L. Structural rearrangements preceding dioxygen formation by the water oxidation complex of photosystem II. *Proc. Natl. Acad. Sci. U.S.A.* **2015**, *112*, E6139−E6147.
(94) Narzi, D.; Capone, M.; Bovi, D.; Guidoni, L. Evolution from S_3 to S_4 states of the oxygen-evolving complex in photosystem II monitored by quantum mechanics/molecular mechanics (QM/MM) dynamics. *Chem.—Eur. J.* **2018**, *24*, 10820−10828.
(95) Kuroda, H.; Kawashima, K.; Ueda, K.; Ikeda, T.; Saito, K.; Ninomiya, R.; Hida, C.; Takahashi, Y.; Ishikita, H. Proton transfer pathway from the oxygen-evolving complex in photosystem II substantiated by extensive mutagenesis. *Biochim. Biophys. Acta, Bioenerg.* **2021**, *1862*, 148329.
(96) Allgöwer, F.; Gamiz-Hernandez, A. P.; Rutherford, A. W.; Kaila, V. R. I. Molecular principles of redox-coupled protonation dynamics in photosystem II. *J. Am. Chem. Soc.* **2022**, *144*, 7171−7180.
(97) Siegbahn, P. E. M. The performance of hybrid DFT for mechanisms involving transition metal complexes in enzymes. *J. Biol. Inorg Chem.* **2006**, *11*, 695−701.
(98) Blomberg, M. R. A.; Borowski, T.; Himo, F.; Liao, R.-Z.; Siegbahn, P. E. M. Quantum chemical studies of mechanisms for metalloenzymes. *Chem. Rev.* **2014**, *114*, 3601−3658.
(99) Cramer, C. J.; Truhlar, D. G. Density functional theory for transition metals and transition metal chemistry. *Phys. Chem. Chem. Phys.* **2009**, *11*, 10757−10816.
(100) Siegbahn, P. E. M.; Himo, F. The quantum chemical cluster approach for modeling enzyme reactions. *Wiley Interdiscip. Rev.: Comput. Mol. Sci.* **2011**, *1*, 323−336.
(101) Ugur, I.; Rutherford, A. W.; Kaila, V. R. I. Redox-coupled substrate water reorganization in the active site of photosystem II-the role of calcium in substrate water delivery. *Biochim. Biophys. Acta, Bioenerg.* **2016**, *1857*, 740−748.
(102) Vinyard, D. J.; Khan, S.; Askerka, M.; Batista, V. S.; Brudvig, G. W. Energetics of the S_2 state spin isomers of the oxygen-evolving complex of photosystem II. *J. Phys. Chem. B* **2017**, *121*, 1020−1025.
(103) Isobe, H.; Shoji, M.; Shen, J.-R.; Yamaguchi, K. Strong coupling between the hydrogen bonding environment and redox chemistry during the S_2 to S_3 transition in the oxygen-evolving complex of photosystem II. *J. Phys. Chem. B* **2015**, *119*, 13922−13933.
(104) Saitow, M.; Becker, U.; Riplinger, C.; Valeev, E. F.; Neese, F. A new near-linear scaling, efficient and accurate, open-shell domain-based local pair natural orbital coupled cluster singles and doubles theory. *J. Chem. Phys.* **2017**, *146*, 164105.
(105) Quagliano, J. V.; Schubert, L. The trans effect in complex inorganic compounds. *Chem. Rev.* **1952**, *50*, 201−260.
(106) Shustorovich, E. M.; Porai-Koshits, M. A.; Buslaev, Y. A. The mutual influence of ligands in transition metal coordination compounds with multiple metal-ligand bonds. *Coord. Chem. Rev.* **1975**, *17*, 1−98.
(107) Burdett, J. K.; Albright, T. A. Trans influence and mutual influence of ligands coordinated to a central atom. *Inorg. Chem.* **1979**, *18*, 2112−2120.
(108) Coe, B. J.; Glenwright, S. J. Trans-effects in octahedral transition metal complexes. *Coord. Chem. Rev.* **2000**, *203*, 5−80.
(109) Linke, K.; Ho, F. M. Water in photosystem II: structural, functional and mechanistic considerations. *Biochim. Biophys. Acta, Bioenerg.* **2014**, *1837*, 14−32.
(110) Ishikita, H.; Saenger, W.; Loll, B.; Biesiadka, J.; Knapp, E.-W. Energetics of a possible proton exit pathway for water oxidation in photosystem II. *Biochemistry* **2006**, *45*, 2063−2071.
(111) Rivalta, I.; Amin, M.; Luber, S.; Vassiliev, S.; Pokhrel, R.; Umena, Y.; Kawakami, K.; Shen, J.-R.; Kamiya, N.; Bruce, D.;

Brudvig, G. W.; Gunner, M. R.; Batista, V. S. Structural-functional role of chloride in photosystem II. *Biochemistry* **2011**, *50*, 6312−6315.
(112) Pal, R.; Negre, C. F. A.; Vogt, L.; Pokhrel, R.; Ertem, M. Z.; Brudvig, G. W.; Batista, V. S. S_0-State model of the oxygen-evolving complex of photosystem II. *Biochemistry* **2013**, *52*, 7703−7706.
(113) Dilbeck, P. L.; Hwang, H. J.; Zaharieva, I.; Gerencser, L.; Dau, H.; Burnap, R. L. The D1-D61N mutation in synechocystis sp. PCC 6803 allows the observation of pH-sensitive intermediates in the formation and release of O_2 from photosystem II. *Biochemistry* **2012**, *51*, 1079−1091.
(114) Debus, R. J. Evidence from FTIR difference spectroscopy that D1-Asp61 influences the water reactions of the oxygen-evolving Mn_4CaO_5 cluster of photosystem II. *Biochemistry* **2014**, *53*, 2941−2955.
(115) Krewald, V.; Retegan, M.; Cox, N.; Messinger, J.; Lubitz, W.; DeBeer, S.; Neese, F.; Pantazis, D. A. Metal oxidation states in biological water splitting. *Chem. Sci.* **2015**, *6*, 1676−1695.
(116) Li, X.; Siegbahn, P. E. M.; Ryde, U. Simulation of the isotropic EXAFS spectra for the S_2 and S_3 structures of the oxygen evolving complex in photosystem II. *Proc. Natl. Acad. Sci. U.S.A.* **2015**, *112*, 3979−3984.
(117) Siegbahn, P. E. M. Computational investigations of S_3 structures related to a recent X-ray free electron laser study. *Chem. Phys. Lett.* **2017**, *690*, 172−176.
(118) Pantazis, D. A. The S_3 state of the oxygen-evolving complex: overview of spectroscopy and XFEL crystallography with a critical evaluation of early-onset models for O-O bond formation. *Inorganics* **2019**, *7*, 55.
(119) Glöckner, C.; Kern, J.; Broser, M.; Zouni, A.; Yachandra, V.; Yano, J. Structural changes of the oxygen-evolving complex in photosystem II during the catalytic cycle. *J. Biol. Chem.* **2013**, *288*, 22607−22620.
(120) Askerka, M.; Wang, J.; Vinyard, D. J.; Brudvig, G. W.; Batista, V. S. S_3 state of the O_2-evolving complex of photosystem II: insights from QM/MM, EXAFS, and femtosecond X-ray diffraction. *Biochemistry* **2016**, *55*, 981−984.
(121) Schuth, N.; Zaharieva, I.; Chernev, P.; Berggren, G.; Anderlund, M.; Styring, S.; Dau, H.; Haumann, M. Kα X-ray emission spectroscopy on the photosynthetic oxygen-evolving complex supports manganese oxidation and water binding in the S_3 state. *Inorg. Chem.* **2018**, *57*, 10424−10430.
(122) de Lichtenberg, C.; Kim, C. J.; Chernev, P.; Debus, R. J.; Messinger, J. The exchange of the fast substrate water in the S_2 state of photosystem II is limited by diffusion of bulk water through channels − implications for the water oxidation mechanism. *Chem. Sci.* **2021**, *12*, 12763−12775.
(123) Drosou, M.; Pantazis, D. A. Redox isomerism in the S_3 state of the oxygen-evolving complex resolved by coupled cluster theory. *Chem.—Eur. J.* **2021**, *27*, 12815−12825.
(124) Nilsson, H.; Rappaport, F.; Boussac, A.; Messinger, J. Substrate-water exchange in photosystem II is arrested before dioxygen formation. *Nat. Commun.* **2014**, *5*, 4305.
(125) Rappaport, F.; Ishida, N.; Sugiura, M.; Boussac, A. Ca^{2+} determines the entropy changes associated with the formation of transition states during water oxidation by photosystem II. *Energy Environ. Sci.* **2011**, *4*, 2520−2524.
(126) Siegbahn, P. E. M. Nucleophilic water attack is not a possible mechanism for O-O bond formation in photosystem II. *Proc. Natl. Acad. Sci. U.S.A.* **2017**, *114*, 4966−4968.
(127) Renger, G. Photosynthetic water oxidation to molecular oxygen: apparatus and mechanism. *Biochim. Biophys. Acta, Bioenerg.* **2001**, *1503*, 210−228.
(128) Eyring, H. The activated complex in chemical reactions. *J. Chem. Phys.* **1935**, *3*, 107−115.
(129) Laidler, K. J.; King, M. C. Development of transition-state theory. *J. Phys. Chem.* **1983**, *87*, 2657−2664.
(130) Truhlar, D. G.; Garrett, B. C.; Klippenstein, S. J. Current status of transition-state theory. *J. Phys. Chem.* **1996**, *100*, 12771−12800.
(131) Siegbahn, P. E. M.; Blomberg, M. R. A. Density functional theory of biologically relevant metal centers. *Annu. Rev. Phys. Chem.* **1999**, *50*, 221−249.
(132) Wang, J.; Askerka, M.; Brudvig, G. W.; Batista, V. S. Crystallographic data support the carousel mechanism of water supply to the oxygen-evolving complex of photosystem II. *ACS Energy Lett.* **2017**, *2*, 2299−2306.
(133) Askerka, M.; Vinyard, D. J.; Brudvig, G. W.; Batista, V. S. NH_3 binding to the S_2 state of the O_2-evolving complex of photosystem II: analogue to H_2O binding during the $S_2 \rightarrow S_3$ transition. *Biochemistry* **2015**, *54*, 5783−5786.
(134) Capone, M.; Narzi, D.; Bovi, D.; Guidoni, L. Mechanism of water delivery to the active site of photosystem II along the S_2 to S_3 transition. *J. Phys. Chem. Lett.* **2016**, *7*, 592−596.
(135) Kim, C. J.; Debus, R. J. Evidence from FTIR difference spectroscopy that a substrate H_2O molecule for O_2 formation in photosystem II is provided by the Ca ion of the catalytic Mn_4CaO_5 cluster. *Biochemistry* **2017**, *56*, 2558−2570.
(136) Kim, C. J.; Debus, R. J. One of the substrate waters for O_2 formation in photosystem II is provided by the water-splitting Mn_4CaO_5 cluster's Ca^{2+} ion. *Biochemistry* **2019**, *58*, 3185−3192.
(137) Pérez-Navarro, M.; Neese, F.; Lubitz, W.; Pantazis, D. A.; Cox, N. Recent developments in biological water oxidation. *Curr. Opin. Chem. Biol.* **2016**, *31*, 113−119.
(138) McEvoy, J. P.; Brudvig, G. W. Water-splitting chemistry of photosystem II. *Chem. Rev.* **2006**, *106*, 4455−4483.
(139) Amin, M.; Kaur, D.; Yang, K. R.; Wang, J.; Mohamed, Z.; Brudvig, G. W.; Gunner, M. R.; Batista, V. Thermodynamics of the S_2-to-S_3 state transition of the oxygen-evolving complex of photosystem II. *Phys. Chem. Chem. Phys.* **2019**, *21*, 20840−20848.
(140) de Lichtenberg, C.; Avramov, A. P.; Zhang, M.; Mamedov, F.; Burnap, R. L.; Messinger, J. The D1-V185N mutation alters substrate water exchange by stabilizing alternative structures of the Mn4Ca-cluster in photosystem II. *Biochim. Biophys. Acta, Bioenerg.* **2021**, *1862*, 148319.
(141) Rapatskiy, L.; Cox, N.; Savitsky, A.; Ames, W. M.; Sander, J.; Nowaczyk, M. M.; Rögner, M.; Boussac, A.; Neese, F.; Messinger, J.; Lubitz, W. Detection of the water-binding sites of the oxygen-evolving complex of photosystem II using W-band ^{17}O electron-electron double resonance-detected NMR spectroscopy. *J. Am. Chem. Soc.* **2012**, *134*, 16619−16634.
(142) Navarro, M. P.; Ames, W. M.; Nilsson, H.; Lohmiller, T.; Pantazis, D. A.; Rapatskiy, L.; Nowaczyk, M. M.; Neese, F.; Boussac, A.; Messinger, J.; Lubitz, W.; Cox, N. Ammonia binding to the oxygen-evolving complex of photosystem II identifies the solvent-exchangeable oxygen bridge (μ-oxo) of the manganese tetramer. *Proc. Natl. Acad. Sci. U.S.A.* **2013**, *110*, 15561−15566.
(143) Lohmiller, T.; Krewald, V.; Sedoud, A.; Rutherford, A. W.; Neese, F.; Lubitz, W.; Pantazis, D. A.; Cox, N. The first state in the catalytic cycle of the water-oxidizing enzyme: identification of a water-derived μ-hydroxo bridge. *J. Am. Chem. Soc.* **2017**, *139*, 14412−14424.

https://doi.org/10.1021/jacs.2c03528
J. Am. Chem. Soc. 2022, 144, 11736−11747